CrossMark

Possible Atmospheric Water Vapor Contribution from Martian Swiss Cheese Terrain

Alex C. Innanen[1] , Margaret E. Landis[2] , Paul O. Hayne[2] , and John E. Moores[1]
[1] Centre for Research in Earth and Space Science, York University, Toronto, ON M3J 1P3, Canada; ainnanen@yorku.ca
[2] Laboratory for Atmospheric and Space Physics, University of Colorado Boulder, Boulder, CO 80303, USA

Abstract

Mars's south polar residual cap (SPRC) is a several-meters-thick CO_2 ice cap with a variety of features, including quasi-circular depressions known as "Swiss cheese" that may expose underlying water ice. Swiss cheese pits have been suggested as a source for the observation of unusually high water vapor during the southern summer of Mars Year (MY) 8 (1969). To evaluate this hypothesis, we map the current extent of Swiss cheese pits to estimate the contribution to atmospheric water vapor from sublimation from the pits. We use data from the Mars Reconnaissance Orbiter Context Camera to map individual features and use the Mars Climate Sounder to obtain surface temperatures to estimate areas of exposed water ice to infer the amount of water vapor sublimated under typical south polar summer atmospheric conditions. We find that there is a negligible impact on atmospheric water vapor from sublimation with the current coverage and temperatures of Swiss cheese terrain (0.2% of the SPRC at an average of ∼161 K). At current typical temperatures, complete removal of residual CO_2 from 99% of the SPRC would be required to sublimate enough water vapor to reproduce the MY 8 observation. However, a modest increase in temperature (∼20 K) could lead to a dramatic increase in sublimation rate, such that only water ice over 2.6% of the SPRC area would recreate the MY 8 observation. >180 K surface water ice has been observed on Mars, but such temperatures are likely transient at the south pole over the past ∼30 Mars years.

Unified Astronomy Thesaurus concepts: Mars (1007); Water vapor (1791); Planetary atmospheres (1244); Polar caps (1273)

1. Introduction

The south polar deposits of Mars consist of a seasonal CO_2 ice cap, which forms during southern fall and winter and retreats in southern spring and summer; a stable, residual CO_2 ice cap (the south polar residual cap (SPRC)), which sits on water-ice bounding layers within a buried CO_2 ice deposit (Phillips et al. 2011; Bierson et al. 2016); and the underlying but more spatially extensive dusty water-ice south polar layered deposits (SPLD). The current stability of the SPRC is linked to the massive CO_2 deposit (Buhler et al. 2020; Buhler & Piqueux 2021). Observations over the past century have suggested that regions on the SPRC have changed significantly enough to be detected in comparisons of Mariner 9, Viking, and Mars Odyssey data, even if some changes are not yet well understood (Piqueux & Christensen 2008).

The SPRC thickness ranges from about 10–14 m to ∼1 m in younger areas, which compose most of the SPRC (Thomas et al. 2009). Also present on both the north and south polar caps are large, spiral troughs. SPRC morphological features include long, asymmetric, parallel depressions known as "fingerprint terrain"; raised mesas; and smaller curl, heart-shaped, and quasi-circular depressions known as "Swiss cheese" pits (Thomas et al. 2009, 2016). Swiss cheese pits apparently record local climatologically recent erosion of the SPRC and exposure of underlying water ice, but their role in altering the abundance of water vapor in the Martian atmosphere, if any, is not well known. The flux of water vapor in and out of the polar regions is a current high-priority science question (Smith et al. 2020).

Swiss cheese pits have flat floors and steep sides and tend to be <500 m in diameter and ∼8 m in depth (Thomas et al. 2000). They grow outward at a rate of a few meters per year (Malin et al. 2001), which could lead to a total resurfacing of the SPRC by Swiss cheese growth every ∼100 yr (Byrne & Ingersoll 2003). They are formed when fractures in the SPRC either widen through sublimation or collapse into pits 1–2 m deep. They continue to grow outward through sublimation of CO_2 from the walls, or through calving blocks from the pit walls (Buhler et al. 2017). The asymmetries in pits are likely due to insolation, with the southern wall receiving more solar radiation than the northern wall (Byrne & Ingersoll 2003).

The southern hemisphere of Mars typically sees a gradual rise in water vapor through the southern spring through transport from the northern hemisphere. The sublimation of the seasonal polar cap later in southern spring leads to an increase of water vapor at high southern latitudes, with a maximum water vapor abundance around $L_s = 290°$. Water vapor abundance begins to decrease around $L_s = 300°$ over the south pole and around $L_s = 330°$ over the entire planet (Montmessin et al. 2017). Whereas the water ice in the SPLD is largely covered by a thick layer of dust (Herkenhoff & Plaut 2000), the water ice of the north polar layered deposits (NPLD) is exposed in its residual cap (Thomas et al. 2000); the NPLD is therefore the main source of seasonal water vapor variation on the planet (Smith 2002). The peak southern summer water vapor abundance is about 20 pr μm, compared to the northern summer's 60–70 pr μm (Trokhimovskiy et al. 2015); however, the southern abundance can vary interannually as much as 10 pr μm (Smith 2004). An exception to this was during the southern summer of Mars Year (MY) 8 (1969), when there was an Earth-based telescopic observation of an unusually high amount of water vapor (45–50 pr μm) above the south pole (Barker et al. 1970). This amount of water vapor during the
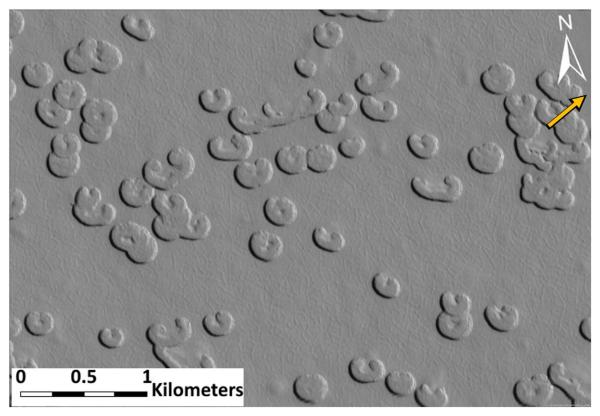
Figure 1. Example Swiss cheese pits from the Murray lab mosaic (Dickson et al. 2018) at 86.9° S, 6.6° W. A variety of different shapes are shown, from more circular features to curl-shaped or branching features. Direction of sunlight is indicated by the yellow arrow.

southern summer has not been observed since, and there is currently no definitive explanation for it. It has been suggested that removal of most or all of the CO_2 ice of the SPRC, exposing water ice that then sublimated, could be responsible for this observation (Jakosky & Barker 1984; Byrne & Ingersoll 2003). While the Barker et al. (1970) observation does have an uncertainty of about 50%, its unusual nature and potential implications for decadal-scale climate variations make it worthwhile to examine with a new data set and to determine whether it is possible to recreate the observed water vapor increase through the expansion of Swiss cheese pits.

This work estimates the magnitude of the impact Swiss cheese pits are likely to have on present-day Martian atmospheric water vapor, and whether these pits represent a plausible explanation for the unusual water vapor observation of MY 8. Our work is motivated by the following questions:

1. How much water vapor is produced from the current configuration of Swiss cheese pits?
2. Is it possible to recreate the MY 8 observation through partial or total removal of CO_2 on the SPRC, and if so, under what conditions?

We present results from mapping Swiss cheese pits and a basic sublimation model to address these questions.

2. Methods

To address our key questions, we mapped the area excavated by Swiss cheese pits on the SPRC using images from the Mars Reconnaissance Orbiter (MRO) Context Camera (CTX) (example features shown in Figure 1). We then used the ratio of smooth-topped CO_2-ice mesas to carved out Swiss cheese

pits, as well as retrievals from MRO's Mars Climate Sounder (MCS) to derive a water-ice surface temperature and from there a sublimation rate, according to detailed explanations below.

2.1. Mapping the Area of Swiss Cheese Pits

The CTX has a resolution of 5–6.5 m pixel^{-1} and is intended to provide context images for other MRO instruments, as well as observe the terrain of Mars (Malin et al. 2007). To map individual Swiss cheese pits on the SPRC, we used the Murray Lab mosaic in ArcMap, a blended mosaic of CTX images with a resolution of 5 m pixel^{-1} (Dickson et al. 2018), in ESRI ArcMap 10.7.1.

In order to identify areas of Swiss cheese terrain (Unit A1 in Thomas et al. 2009), we used the Thomas et al. (2009) unit map (Figure 1(a) in Thomas et al. 2009) overlaid on the CTX mosaic. While a newer unit map exists in Thomas et al. (2016), there is little difference in the extent and locations of the A1 unit, which we used to map Swiss cheese pits. The unit map shows distinct areas of Swiss cheese terrain, but a GIS-software compatible shapefile for either the Thomas et al. (2009) or Thomas et al. (2016) unit maps was unavailable. We traced the figure in ArcMap to create sites (cyan outlines in Figure 3) in which we mapped individual pits. Of the sites identified by this method, several smaller sites were excluded because of the uncertainty in determining their exact margins from the Thomas et al. (2009) map due to resolution issues.

Polygons were drawn in ArcMap to map the Swiss cheese pits within the identified sites. For sites less than 10 km^2, the entire site was mapped, but in order to save time, only about 25% of sites larger than 10 km^2 were mapped in order to derive

a representative sample of Swiss cheese pit area versus high-standing CO_2 ice.

Some of the Swiss cheese pits contain interior raised areas. These are high-standing areas assumed to be remnants of the SPRC (Buhler et al. 2017) and were mapped and excluded from the final total area of Swiss cheese pits. This allowed us to determine a fraction of terrain carved out of the SPRC by negative topography features within each Swiss cheese site.

2.2. Surface Temperatures

We used surface temperature retrievals from the MCS to determine secondary temperatures present within a site that represents potential exposed water ice mixed in with the surrounding CO_2 ice within an MCS observation footprint. As MCS on-planet measurements have a footprint of 6×6 km^2 (e.g., Hayne et al. 2012), we only looked at sites that were greater than 20 km^2 to ensure that the Swiss cheese terrain filled most of the footprint, as well as being at least 6 km away from any troughs to eliminate any thermal effects from their starkly different albedo from the SPRC surfaces. The MCS surface temperature retrieval (Piqueux et al. 2016, and references therein) provides a 32 μm brightness temperature of the whole scene, and in order to calculate the CO_2 frost temperature (T_{CO_2}) within the scene, the MCS surface pressure record (P_{surf}) was also used:

$$T_{CO_2} = \frac{-\beta}{\ln(P_{surf}) - \alpha}, \qquad (1)$$

where α and β are fit constants to experimental data with values $\alpha = 23.3494$ and $\beta = 3182.48$ (James et al. 1992), and P_{surf} is in mbar. While other relations exist (e.g., Span & Wagner 1996), we have chosen to use this one to be consistent with Piqueux et al. (2016). A bolometric, graybody scene emissivity could then be determined using the expression

$$\epsilon_{scene} = \frac{T_b^4}{T_{CO_2}^4}, \qquad (2)$$

where T_b is the retrieved MCS brightness temperature. Any scene emissivity less than 1 was assumed to contain only CO_2 ice, while a scene emissivity greater than 1 indicated the presence of some other material in the scene, as a single-component CO_2 surface cannot physically have an emissivity greater than 1. Variation in emissivities between 0 and 1 is assumed to be due to variation in CO_2 particle size (Gary-Bicas et al. 2020). For scenes with $\epsilon_{scene} > 1$, the secondary material is assumed to be water ice based on the following conclusions of previous work. Byrne & Ingersoll (2003) demonstrated that a model of an H_2O ice layer underneath $\sim$10 m of CO_2 best matches observations of Swiss cheese feature formation and expansion. Additionally, CRISM data have shown water ice in the walls and floors of some Swiss cheese pits (Cartwright et al. 2022). Finally, our derived MCS water-ice temperatures (Section 3) are for the most part in the same range as retrieved THEMIS water-ice temperatures for Swiss cheese terrain, presented in Byrne & Ingersoll (2003), demonstrating cross data set consistency in our inferred temperatures.

With the retrieved surface brightness temperatures and subpixel Swiss cheese areas, a linear subpixel mixing model was then used to determine what temperature of the water ice would be required to reproduce the retrieved MCS surface temperatures. The brightness temperature of the scene is calculated first by determining the total emitted radiance from CO_2 and H_2O components within the MCS footprint:

$$R_\lambda = f\epsilon_{H_2O}B_\lambda(T_{H_2O}) + (1 - f)\epsilon_{CO_2}B_\lambda(T_{CO_2}), \qquad (3)$$

where R_λ is the retrieved scene radiance; f is the fraction of the scene taken up by water ice; ϵ_{H_2O} is the emissivity of water ice (0.987; Warren et al. 1990); $B_\lambda(T_{H_2O})$ is the blackbody radiance from water ice; ϵ_{CO_2} is the CO_2 emissivity, for which we use a value of 0.9 based on MCS observations of regions of pure CO_2 on the SPRC at this season (e.g., Gary-Bicas et al. 2020); and $B_\lambda(T_{CO_2})$ is the blackbody radiance from CO_2 ice at the known frost point, T_{CO_2}. An upper bound on the fraction of water ice present was taken as the mapped fraction of Swiss cheese pits within a given scene. While the emissivity does vary over the season by a few percent (Gary-Bicas et al. 2020), when we performed a sensitivity analysis and varied the CO_2 emissivity by ± 0.1, the corresponding differences in calculated water-ice temperature were small ($\sim \pm 1$ K).

From our derived water-ice temperature (T_{H_2O}), we can then determine a sublimation rate of the exposed water ice. The saturation vapor pressure (SVP; P_s) at the ice−atmosphere boundary for a given temperature of water ice is given by the Clausius−Clapeyron equation (based on Equation (5) in Schorghofer 2008):

$$P_s = P_t \exp\left[-\frac{\Delta H}{R}\left(\frac{1}{T_{H_2O}} - \frac{1}{T_t} \right) \right], \qquad (4)$$

where P_t is the triple point pressure of water (611 Pa), ΔH is the change in enthalpy (51.058 kJ mol^{-1}), R is the universal gas constant (8.3145×10^{-3} kJ mol^{-1} K^{-1}), and T_t is the triple point temperature of water (273.16 K). We can then use the SVP to compute a mass-loss rate ($\bar{J}$) into vacuum in kg m^{-2} s^{-1}:

$$\bar{J} = P_s \sqrt{\frac{2m}{\pi k_B T_{H_2O}}}, \qquad (5)$$

where m is the mass of one water molecule (2.988×10^{-26} kg) and k_B is the Boltzmann constant (1.381×10^{-23} m^2 kg s^{-1} K^{-1}). CO_2 surface pressure may impact the mass-loss rate (e.g., Dundas & Byrne 2010); however, we are interested in an upper limit water vapor production. As a result, we use this simplified model of sublimation into vacuum.

We use our mapped Swiss cheese area as an observational constraint on f in Equation (3). With this and the calculated mass flux, we can estimate the mass loss from Swiss cheese terrain in its currently observed configuration, assuming a sufficiently dry Martian atmosphere that instantly transports away sublimated water vapor (e.g., Dundas & Byrne 2010). This assumption is justified in Section 3. This is roughly equivalent to assuming constant zero partial pressure of water vapor in the atmospheric surface layer (Shorghofer & Aharonson 2005). This framework can then be extended to a situation in which the entire SPRC is carved out by Swiss cheese pits, exposing water ice. The MY 8 observation saw 45–50 pr μm of water vapor above the south pole (Barker et al. 1970), approximately twice the typical southern hemisphere peak for water vapor abundance.

We can determine the water vapor column abundance (PW, precipitable water) from the mass of water vapor released

(m_{H_2O}) using the expression

$$PW = \frac{1}{A}\left(\frac{m_{H_2O}}{\rho_{H_2O}}\right), \qquad (6)$$

where A is the area of interest and ρ_{H_2O} is the density of liquid water. We can also determine the partial pressure of the sublimated water vapor using

$$P_{H_2O} = \frac{m_{H_2O}}{A}g, \qquad (7)$$

where g is the acceleration due to gravity (3.71 m s^{-2} on Mars). This quantity can be compared with the SVP of water vapor in the atmosphere:

$$SVP = 10^{-\frac{2663.5}{T}+12.537}, \qquad (8)$$

adapted from Equation (1) in Marti & Mauersberg (1993), where T is the atmospheric temperature just above the surface. If the partial pressure of the sublimated water vapor is much less than the SVP, it is reasonable to assume that the atmosphere is dry and that downward flux of water vapor is negligible. If the partial pressure is greater than the SVP, then there will likely be condensation of water molecules back onto the surface of the SPRC. This is an important consideration in supporting our assumption that the Martian atmosphere is essentially dry with respect to water vapor in the sublimation rate calculation.

3. Results

We mapped Swiss cheese pits in a total of 83 sites identified from unit A1 of the Thomas et al. (2009) unit map as outlined in Section 2.1, for a total site area of 1 627.8 km^2. The smallest site area was 0.7 km^2, and the largest was 472.2 km^2. Of these sites, four contained features that did not resemble typical Swiss cheese terrain and were excluded from mapping. An example of a rejected site is presented in Figure 2.

As all four of these sites also fell below the minimum size for temperature retrieval, and most were near troughs, their exclusion did not impact the sublimation calculations. The total area of the SPRC is 79,159 km^2 (Thomas et al. 2016). The total mapped area of Swiss cheese pits was 184.2 km^2, or 0.232% of the total area of the SPRC. The average ratio of the area contained within Swiss cheese pits to their surrounding high-standing terrain within unit A1 sites was 42.8%, varying from 11.5% to 85.0%.

Twenty sites had areas greater than 20 km^2, which was our minimum surface area for MCS retrievals. At smaller sites, the 6×6 km^2 MCS footprint could contain too much non–Swiss cheese terrain. Of these 20 sites, 14 were sufficiently far from a trough and had more than one surface temperature retrieval from MCS. Troughs have a significantly different albedo from the surrounding SPRC, which means that we cannot assume that they have the same thermal properties as pure CO_2 ice. Thus, we avoided retrievals that may have included troughs in the footprint. These 14 sites were further narrowed down to five that contained observations indicative of the presence of water ice, as shown in Figure 3.

Subpixel mixing models were created for each of the sites using the mean summertime CO_2-ice temperatures of the respective sites (T_{CO_2} in Equation (3)). Sites 2, 4, and 5 have average CO_2-ice temperatures of 144.3 K, while site 3 has a CO_2-ice temperature of 143.3 K and site 1 has a CO_2-ice temperature of 146 K. While these average CO_2 temperatures

were used in creating the subpixel mixing plots (shown in Figure 4), the CO_2-ice temperatures calculated from retrieved surface pressures for each observation were used in calculating that observation's water-ice temperature. However, there was only at most a few-kelvin difference between these CO_2-ice temperatures, and using an average temperature does not significantly impact the plots. The majority of the derived water-ice temperatures fall between 150 and 180 K. As described in Section 2, these temperatures (150–180 K) agree with Thermal Emission Imaging System (THEMIS) observations presented by Byrne & Ingersoll (2003) of Swiss cheese depression floors (Figure 3 in Byrne & Ingersoll 2003).

There are five inferred water-ice temperatures above 190 K, much higher than other inferred water-ice temperatures, that correspond to scene emissivities (ϵ_{scene}, from Equation (2)) of $\sim$1.5 and above. It is unclear what is causing these unusually high inferred temperatures. The retrieved MCS temperature and pressure errors for these higher temperatures all fall within the range of variations seen in the nominal observations. There does not appear to be a temporal connection to these observations, as they are distributed throughout the southern summer and the 6 Mars years over which the observations are taken (Table 1). While one of these observations falls in MY 34, after the global dust storm, so too do several observations resulting in more typical temperatures. We examined retrieved MCS dust optical depths for the Swiss cheese sites and were unable to find a correlation between optical depth and brightness temperature. While such a correlation may exist, this does not appear to be the reason for these higher inferred temperatures. Additionally, none of the cutoff elevations of the retrievals are sufficiently high to indicate unreliable retrievals, and thus it is unlikely that these higher temperatures are the result of instrumental artifacts (S. Piqueux 2021, personal communication).

We chose to include these points for completeness in our calculations, but we acknowledge that they are outliers without clear cause from the retrieved temperature data. Because of the large thermal gradient between these high water-ice temperatures and the surrounding CO_2 ice (between 143 and 146 K), it is unlikely that these temperatures are sustainable over the southern summer; however, modeling beyond the scope of this paper would be required to understand under which thermal conditions these water-ice temperatures could be sustained.

The water-ice temperatures calculated for each data point are the lower bound water-ice temperature assuming that all area carved out by Swiss cheese pits exposes water ice (shown in Table 1). These temperatures are in the range of $L_s = 255°$–$351°$ (late southern spring through summer) from MY 28 to 34. There does not appear to be any connection between solar longitude and water-ice temperature or any indication that years of global dust storms had an impact, although with a total of only 24 total retrievals over 6 Martian years, there might also be a lack of sufficient temporal coverage to be able to rule out effects from planet-encircling dust events entirely. From the derived water-ice temperatures it is possible to calculate a mass-loss rate using Equation (5). These are also presented in Table 1.

Excluding the water-ice temperatures greater than 190 K, there is an average water-ice temperature of $\sim$161 K, which corresponds to a mass-loss rate of 2.8×10^{-7} kg m^{-2} s^{-1}. Under the current configuration of Swiss cheese pits and assuming that the total low-standing area carved out by Swiss
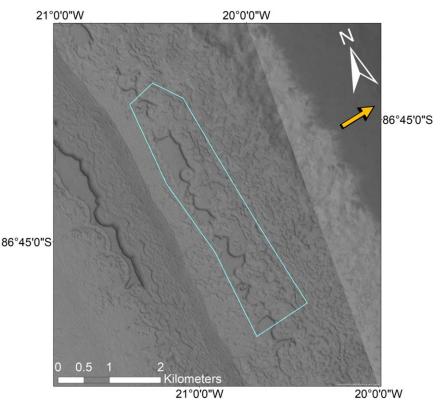
Figure 2. An example site that was rejected for mapping. In addition to being too near to a trough (the dark feature in the upper right corner) for temperature retrieval, it was difficult to identify where recognizable Swiss cheese pits graded into the non–Swiss cheese nearby terrain. Direction of sunlight is indicated by the yellow arrow.

cheese (184.2 km^2) is exposing water ice and sublimating over the whole southern summer (154 sols), we have an upper limit on water vapor production of 7.0×10^8 kg of water vapor, which mixed over all of Mars' atmosphere would produce 4.9×10^{-3} pr μm or a partial pressure of 1.8×10^{-5} Pa of water vapor.

Figure 5 shows the water vapor abundance produced over the range of derived water-ice temperatures for the current configuration of Swiss cheese pits. Changes of tens of kelvin can result in large changes in the amount of water vapor produced. It is unlikely that the higher water-ice temperatures are sustainable over the entire southern summer, which sees variation over the season. Looking at our nominal range of water-ice temperatures under current Swiss cheese conditions, we see a maximum abundance of water vapor produced of 70.2×10^{-3} pr μm, which corresponds to a partial pressure of 2.6×10^{-4} Pa.

Taking an average MCS-retrieved near-surface atmospheric temperature of 220 K for our points of interest, we computed the SVP for the southern summer atmosphere of 2.7 Pa. Since the partial pressures produced by Swiss cheese pits are four to five orders of magnitude less than the SVP, the release of water vapor from Swiss cheese pits alone will not cause the atmosphere to reach saturation, and there will be negligible downwelling flux. Our assumption of a dry atmosphere is therefore a reasonable approximation in this case.

Both the average $(4.9 \times 10^{-3}$ pr μm$)$ and maximum $(70.2 \times 10^{-3}$ pr μm$)$ quantities of water vapor produced are extremely small compared to the average summer abundance seen in the southern hemisphere, so it is unlikely that the current configuration of Swiss cheese pits contributes substantially to the current overall atmospheric water vapor. In

addition, the currently observed configuration of Swiss cheese pits on the SPRC surface could not have produced enough vapor to explain the 1969 observation.

While these results show that the current Swiss cheese extent does not have a large effect on global atmospheric water vapor, this raises the question of how extensive the Swiss cheese terrain would need to be to match the Barker et al. (1970) observation. The MY 8 observation saw a globally averaged abundance of $45-50$ pr μm, $\sim$2.5 times the average southern summer abundance of 20 pr μm (Trokhimovskiy et al. 2015; Pankine 2022). While recent work has shown that the southern water vapor maximum could be as high as 35 pr μm (Knutsen et al. 2022), we are choosing to use 20 pr μm as our nominal water vapor abundance value, as it is within the observed variation of southern summer water vapor abundances. Assuming that 20 pr μm of water vapor is already present in the southern summer, we quantified the amount of Swiss cheese surface area that would produce the remaining 30 pr μm in the MY 8 observation.

To do this, we assume the same sublimation period and similar surface temperatures as calculated for the present-day case. At a temperature of 173 K, the area of water ice exposed by Swiss cheese pits needs to increase by a factor of 427.2 to a total area of 78,690 km^2, or 99% of the total area of the SPRC. The lower limit of derived water-ice temperatures, 149 K, which produces 2.4×10^{-4} pr μm of water vapor, requires an increase of Swiss cheese area by a factor of 1.2×10^5, or a total area of 2.3×10^7 km^2, over 250 times the area of the SPRC. The sensitivity of vapor production to temperature suggests that a relatively minor (on order $\sim$10 K) warming of water ice could have a significant impact on the total vapor generated by Swiss cheese pits, although mechanisms leading
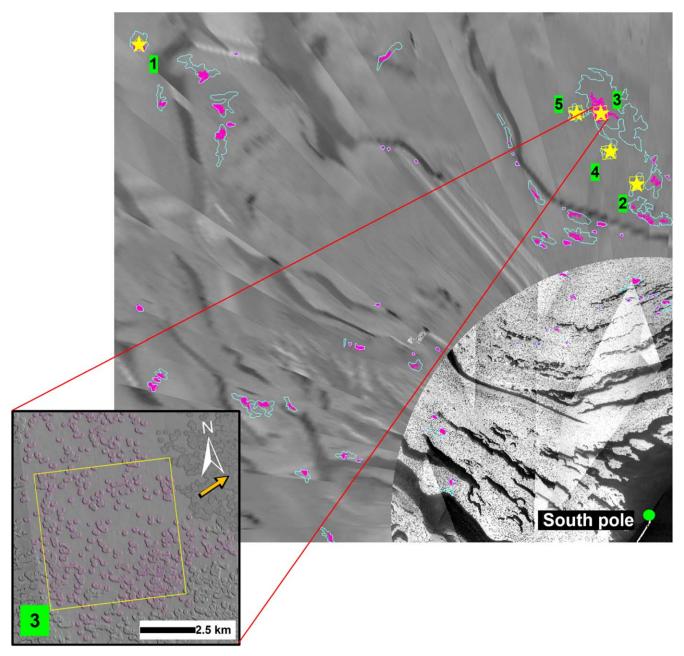
Figure 3. CTX Mosaic of the SPRC with mapped sites of Swiss cheese terrain. Cyan indicates a site of Swiss cheese terrain, with magenta being individual mapped Swiss cheese pits within these sites. Yellow stars indicate sites that suggest the presence of water ice, with their site numbers. The south pole is indicated by the green circle. The inset shows a close-up of site 3, with individually mapped Swiss cheese pits shown, and with the yellow box showing the surface area of an MCS footprint (6×6 km^2). Direction of sunlight is indicated by the yellow arrow.

to this warming are not well known. However, if the outlier temperatures are reasonable representations of temperature that do occur for some fraction of exposed water ice, then it could be possible to get a higher sublimation rate at least for some part of the season. One possibility is that the ~170 K temperatures are a mixture of remnant, nonseasonal CO_2 frost and exposed water ice, and that at some time in the geologic past removal of remnant CO_2 ice could raise the Swiss cheese pit temperature sufficiently for closer to ~200 K water-ice temperatures.

We can conclude that higher-temperature water ice could be responsible for the addition of 30 pr μm of water ice to the Martian atmosphere as a likely upper limit of reasonable vapor production. However, the H_2O ice temperatures closer to the

lower end of our MCS-derived values are not sufficient to produce that amount of water vapor from Swiss cheese terrain on the SPRC, given the magnitude of the area required.

4. Discussion

We set out to answer two questions about water vapor production from Swiss cheese terrain: how much water vapor is currently produced, and whether it is possible to recreate the MY 8 water vapor observation through CO_2 removal by Swiss cheese terrain. At the retrieved nominal temperatures, the current configuration of Swiss cheese terrain does not produce enough water vapor to be significant in terms of the total southern summer water vapor abundance of ~20 pr μm
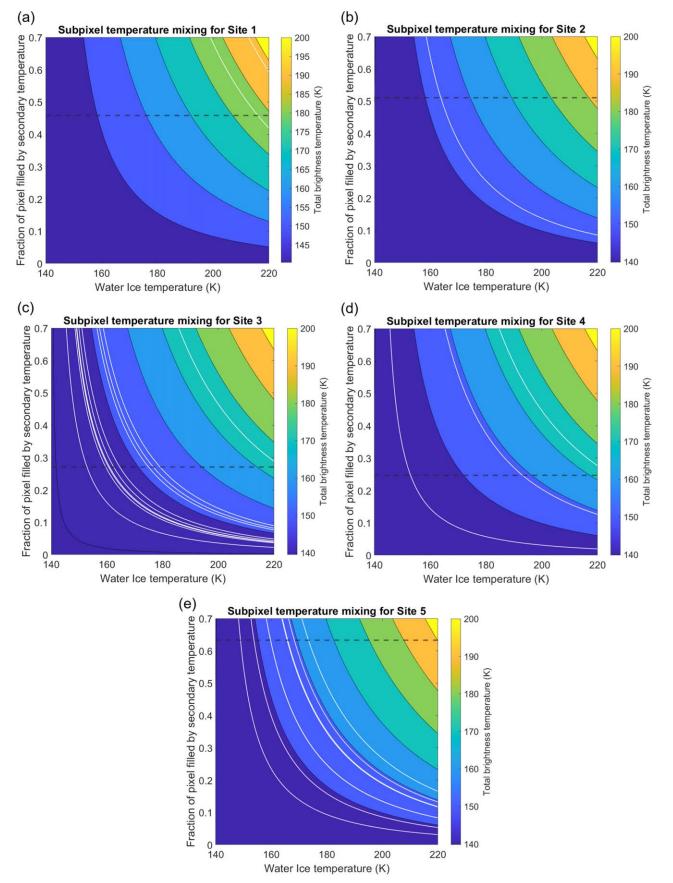
Figure 4. Subpixel temperature mixing plots for Swiss cheese terrain sites with identified water ice. White contour lines represent MCS retrieved brightness temperatures, and the dashed horizontal line represents the mapped fraction of Swiss cheese pits. The intersection of these two lines gives the secondary (water-ice) temperature for that fraction of exposed water ice. The following reference CO_2-ice temperatures were used, based on mean summer temperature: (a) 146 K, (b) 144.3 K, (c) 143.3 K, (d) 144.3 K, (e) 144.3 K.

Table 1
Calculated Water-ice Temperatures and Corresponding Mass-loss Rates of Swiss Cheese Sites

Site ID	MY	L_s (deg)	Water-ice Temperature (K)	Mass-loss Rate (kg m^{-2} s^{-1})
1	29	295.59	232.005	27.6×10^{-3}
1	32	285.07	215.907	4.0×10^{-3}
2	31	334.74	164.190	5.9×10^{-7}
3	28	329.68	158.162	1.4×10^{-7}
3	30	309.76	154.984	6.6×10^{-8}
3	30	328.43	157.840	1.3×10^{-7}
3	31	349.46	150.688	2.2×10^{-8}
3	31	300.13	155.553	7.6×10^{-8}
3	31	329.09	172.066	3.2×10^{-6}
3	32	310.79	169.177	1.7×10^{-6}
3	33	254.83	170.338	2.2×10^{-6}
3	34	328.21	156.399	9.3×10^{-8}
3	34	335.05	212.815	2.7×10^{-3}
4	32	347.08	154.164	5.3×10^{-8}
4	32	316.08	225.160	12.5×10^{-3}
4	33	292.02	193.429	1.5×10^{-4}
5	30	324.35	165.781	8.4×10^{-7}
5	31	306.26	168.260	1.4×10^{-6}
5	31	319.95	173.238	4.0×10^{-6}
5	31	332.02	165.478	7.8×10^{-7}
5	31	351.52	149.100	1.4×10^{-8}
5	34	284.67	153.794	4.8×10^{-8}
5	34	323.56	158.988	1.8×10^{-7}
5	34	330.97	159.687	2.1×10^{-7}

(Pankine 2022). Furthermore, at the highest of the reasonable inferred water-ice temperatures (173 K), 99% of the SPRC would need to be carved out by Swiss cheese terrain in order to sublimate 30 pr μm and bring the total atmospheric water vapor up to levels seen in the MY 8 southern summer (Barker et al. 1970). Given current observations of the growth of Swiss cheese terrain, which would resurface the SPRC every ~100 Martian years (Byrne & Ingersoll 2003), and with the current coverage of the SPRC by Swiss cheese terrain, we would not expect to see such a spike in water vapor abundance currently, or even in the coming years.

A remaining question about the thermal conditions of the Swiss cheese terrain is the true temperatures of the potential water ice in their interiors and evidenced by the five unusually high water-ice temperatures previously reported here. There are relatively few of them, compared to the clustering of data between 150 and 175 K, leading to our classifying them as outliers. However, it is unlikely that these temperatures are nonphysical. Expanded observations of the Swiss cheese terrain in season and local time could shed light on the nature and cause of these warmer inferred water-ice temperatures.
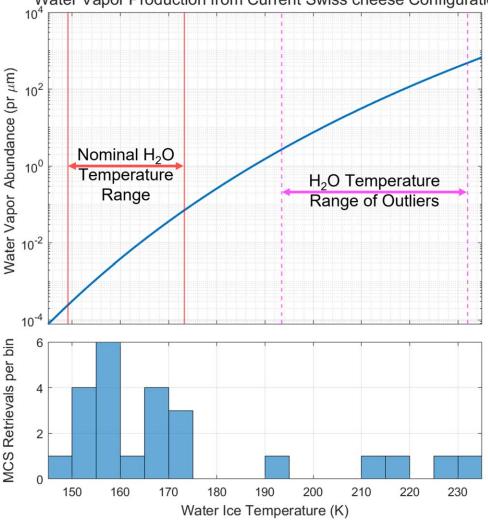
Using these higher values in our water vapor abundance calculation, at the lowest end, 193.4 K, we see a release of 2.7 pr μm over the entire southern summer from the current arrangement of Swiss cheese terrain. However, as we move to the higher values, we quickly reach and exceed the total water vapor abundance seen in MY 8, even with only 0.2% of the SPRC exposing water ice. This supports our assumption that while these >200 K temperatures may exist transiently, they cannot be sustained throughout the southern summer without significantly affecting the total amount of water vapor in the atmosphere. Conversely, if conditions did change from those

currently observed by MCS such that continuous >200 K water-ice temperatures were possible for the Swiss cheese pits during south polar summer, this would produce a detectable change in atmospheric water vapor. Mars has been one of the most continuously monitored planets, aside from Earth, for the past two decades, and no such change has been detected. Many instruments have detection limits precise enough that this change would be easily observable: the Thermal Emission Spectrometer (Christensen et al. 1992) on board the Mars Global Surveyor; the Planetary Fourier Spectrometer (Formisano et al. 2005), Observatoire pour la Minéralogie, l'Eau, les Glaces et l'Activité (Bibring et al. 2004), and the Spectroscopy for the Investigation of the Characteristics of the Atmosphere of Mars instrument (Korablev et al. 2006) on board Mars Express; the Compact Reconnaissance Imaging Spectrometer for Mars (Murchie et al. 2007) on board MRO; and the Nadir and Occultation for Mars Discovery instrument (Vandaele et al. 2018) on board the Trace Gas Orbiter. As such, a significant increase in atmospheric water vapor has not been detected since 1969, either telescopically or from orbiting atmospheric monitoring spacecraft; it is unlikely that these temperatures are widespread or persist throughout a significant amount of the southern summer.

However, at the lowest of these outlier values (193.4 K), there needs to only be an increase in surface area of a factor of 11.2 in order to sublimate 30 pr μm of water vapor at this temperature. This is a total area of exposed water ice of 2054.9 km^2, about 2.6% of the total surface area of the SPRC.

There is the potential that our derived water-ice temperatures are underestimates. It is possible to achieve surface water-ice temperatures in excess of 200 K (e.g., Bapst et al. 2018). It is also possible that the Swiss cheese floors are not entirely exposed water ice, but are instead partially frosted by CO_2. If the MCS observations contain periods of warmer water-ice temperatures, or warmer temperatures overall, this would decrease the total area of Swiss cheese pits needed to recreate the MY 8 observation. On the other hand, if MCS observations contained continually much higher temperatures (>200 K), we would expect to be seeing large spikes in southern summer water vapor production, which has not been observed in almost 30 Mars years. This leads to the conclusion that it is likely that the temperature of the exposed water ice is consistently <200 K, and any >200 K temperatures observed are likely transient enough that they do not substantially increase the total mass of sublimated water vapor.

It is possible that conditions such as widespread and persistent higher water-ice temperatures, greater surface area of water ice exposed by Swiss cheese pits, or some combination of the two could be responsible for the MY 8 observation. However, these parameters are not typical of the SPRC in the present day, which is supported by the lack of a similar observation in the years since MY 8. While images of the SPRC over the past decades do show significant changes and periods of removal and deposition (Piqueux & Christensen 2008), the reason for these changes in the SPRC is likely a combination of seasonal and interannual processes. Observations another 30 MY in the future, if the predictions of Byrne & Ingersoll (2003) are correct about the rate of Swiss cheese retreat, may show different enough conditions to test this hypothesis further.

Figure 5. Water vapor production from the current configuration of Swiss cheese pits. A histogram of derived MCS water-ice temperature values shows a clustering of temperatures between 145 and 175 K, as well as the five higher "outlier" values.

5. Conclusions

The aim of this work was to determine an upper bound on current water vapor contributions from the Swiss cheese pits of the SPRC and use these constraints to determine what area of Swiss cheese terrain would be required to replicate the MY 8 observation. If that area was much greater than the total area of the SPRC under our upper limit assumptions, the contribution of water ice exposed by Swiss cheese pits can be ruled out as a feasible source of vapor in the MY 8 observation. If not, Swiss cheese terrain could plausibly be an important source of additional atmospheric water vapor.

We mapped the current configuration of Swiss cheese pits, which account for around 0.2% of the total area of the SPRC at present. MCS temperature retrievals of Swiss cheese sites were indicative of the presence of exposed water ice in late southern spring and summer. We determined an upper limit on water vapor sublimation from the current configuration of Swiss cheese pits, assuming that the entire mapped area of pits exposes water ice that sublimated throughout the southern summer season, and found that the globally averaged water vapor abundance produced at maximum is 70.2×10^{-3} pr μm,

which is not enough to have an appreciable impact on global atmospheric water vapor.

In order to bring this maximum vapor production up to levels seen in the MY 8 observation, the area of water ice exposed by Swiss cheese needs to increase to 99% of the total area of the SPRC, if we assume current typical temperatures observed by MCS. If we use the higher, >200 K temperatures, it is possible to recreate or even surpass the MY 8 observation with much lower surface area, but we can discount this owing to the lack of similar increases in the amount of atmospheric water vapor since the MY 8 southern summer. It is therefore unlikely that the Swiss cheese pits alone could have produced the anomalous water vapor unless their temperatures were unexpectedly high.

MCS data are archived on the PDS Atmospheres node (https://atmos.nmsu.edu/data_and_services/atmospheres_data/MARS/mcs.html).

Shapefiles for this project are archived at https://doi.org/10.5683/SP3/RK8XTQ.

The authors thank the Mars Reconnaissance Orbiter project and the Mars Climate Sounder team, particularly Sylvain Piqueux for discussion of the temperature retrievals.

ORCID iDs

Alex C. Innanen ● https://orcid.org/0000-0002-4059-2296
Margaret E. Landis ● https://orcid.org/0000-0001-7321-2272
Paul O. Hayne ● https://orcid.org/0000-0003-4399-0449
John E. Moores ● https://orcid.org/0000-0001-9435-1095

References

Bapst, J., Byrne, S., & Brown, A. J. 2018, Icar, 308, 15
Barker, E. S., Schorn, R. A., Woszczyk, A., Tull, R. G., & Little, S. J. 1970, Sci, 170, 1308
Bibring, J. P., Soufflot, A., Berthé, M., et al. 2004, in ESA Special Publication, Vol. 1240, Mars Express: the Scientific Payload, ed. A. Wilson & A. Chicarro (Noordwijk: ESA), 37
Bierson, C. J., Phillips, R. J., Smith, I. B., et al. 2016, GeoRL, 43, 4172
Buhler, P. B., Ingersoll, A. P., Ehlmann, B. L., Fassett, C. I., & Head, J. W. 2017, Icar, 286, 69
Buhler, P. B., Ingersoll, A. P., Piqueux, S., Ehlmann, B. L., & Hayne, P. O. 2020, NatAs, 4, 364
Buhler, P. B., & Piqueux, S. 2021, JGRE, 126, e06759
Byrne, S., & Ingersoll, A. P. 2003, Sci, 299, 1051
Cartwright, S. F. A., Calvin, W. M., Seelos, K. D., & Seelos, F. P. 2022, JGRE, in press (doi:10.1029/2022JE007372)

Christensen, P. R., Anderson, D. L., Chase, S. C., et al. 1992, JGR, 97, 7719
Dickson, J., Kerber, L., Fassett, C., & Ehlmann, B. L. 2018, LPSC, 49, 2480
Dundas, C. M., & Byrne, S. 2010, Icar, 206, 716
Formisano, V., Angrilli, F., Arnold, G., et al. 2005, P&SS, 53, 963
Gary-Bicas, C. E., Hayne, P. O., Horvath, T., et al. 2020, JGRE, 125, e06150
Hayne, P. O., Paige, D. A., Schofield, J. T., et al. 2012, JGRE, 117, E08014
Herkenhoff, K. E., & Plaut, J. J. 2000, Icar, 144, 243
Jakosky, B. M., & Barker, E. S. 1984, Icar, 57, 322
James, P. B., Kieffer, H. H., & Paige, D. A. 1992, in Mars, ed. H. H. Kieffer (Tucson, AZ: Univ. Arizona Press), 934
Knutsen, E. W., Montmessin, F., Verdier, L., et al. 2020, JGRE, 127, e07252
Korablev, O., Bertaux, J.-L., Fedorova, A., et al. 2006, JGRE, 111, E09S03
Malin, M. C., Bell, J. F., Cantor, B. A., et al. 2007, JGRE, 112, E05S04
Malin, M. C., Caplinger, M. A., & Davis, S. D. 2001, Sci, 294, 2146
Marti, J., & Mauersberger, K. 1993, GeoRL, 20, 363
Montmessin, F., Smith, M. D., Langevin, Y., Mellon, M. T., & Fedorova, A. 2017, in The Water Cycle, ed. R. M. Haberle et al. (Cambridge: Cambridge Univ. Press), 338
Murchie, S., Arvidson, R., Bedini, P., et al. 2007, JGRE, 112, E05S03
Pankine, A. A. 2022, Icar, 379, 114975
Phillips, R. J., Davis, B. J., Tanaka, K. L., et al. 2011, Sci, 332, 838
Piqueux, S., & Christensen, P. R. 2008, JGRE, 113, E02006
Piqueux, S., Kleinböhl, A., Hayne, P. O., et al. 2016, JGRE, 121, 1174
Schorghofer, N. 2008, ApJ, 682, 697
Shorghofer, N., & Aharonson, O. 2005, JGRE, 110, E05003
Smith, I. B., Hayne, P. O., Byrne, S., et al. 2020, P&SS, 184, 104841
Smith, M. D. 2002, JGRE, 107, 5115
Smith, M. D. 2004, Icar, 167, 148
Span, R., & Wagner, W. 1996, JPCRD, 25, 1509
Thomas, P. C., Calvin, W., Cantor, B., et al. 2016, Icar, 268, 118
Thomas, P. C., James, P. B., Calvin, W. M., Haberle, R., & Malin, M. C. 2009, Icar, 203, 352
Thomas, P. C., Malin, M. C., Edgett, K. S., et al. 2000, Natur, 404, 161
Trokhimovskiy, A., Fedorova, A., Korablev, O., et al. 2015, Icar, 251, 50
Vandaele, A. C., Lopez-Moreno, J.-J., Patel, M. R., et al. 2018, SSRv, 214, 80
Warren, S. G., Wiscombe, W. J., & Firestone, J. F. 1990, JGR, 95, 14717